Theor Chem Acc (2009) 124:395–408
DOI 10.1007/s00214-009-0629-6

REGULAR ARTICLE

Electronic structure and optical properties of chelating heteroatomic conjugated molecules: a SAC-CI study

Yun-Peng Lu · Masahiro Ehara

Received: 30 June 2009 / Accepted: 21 August 2009 / Published online: 3 September 2009

Abstract The electronic structure and optical properties of 13 chelating heteroatomic conjugated molecules such as pyridine, benzoxazole, and benzothiazole derivatives, which are used as C–N ligands in organometallic compounds, have been investigated. The geometries of the ground and first excited states were obtained by the DFT and CIS methods, respectively, followed by the SAC-CI calculations of the transition energies for absorption and emission. For six compounds whose experimental data are available, the SAC-CI calculations reproduced the experimental values satisfactorily with deviations of less than 0.3 eV for absorption and 0.1 eV for emission except for benzoxazoles. For other molecules, the theoretical absorption and emission spectra were predicted. The lowest $\pi\pi^*$ excited-state geometries was calculated to be planar for most of the molecules with two or three conjugated rings connected by single bond. The geometry change due to the $\pi\pi^*$ excitation was qualitatively interpreted by electrostatic force theory based on SAC/SAC-CI electron density difference. The excitations are relatively localized in the central region and in the lowest $\pi\pi^*$ excited state, the inter-ring single bond shows large change, with a contraction of 0.05–0.09 Å. The present calculations provide reliable information regarding the energy levels of these chelating heteroatomic conjugated compounds.

Keywords Ab initio · SAC-CI · Heteroatomic conjugated molecules · Optical properties · Electronic structure

1 Introduction

Chelating heteroatomic conjugated molecules, such as pyridine, benzoxazole, and benzothiazole derivatives, are technologically important compounds. An increasing research focus for heteroatomic conjugate molecules is their application in the area of organic optoelectronic materials, such as photoconducting materials [1], liquid crystals [2], and fluorophores [3–6]. Meanwhile, heteroatomic conjugated molecules have been widely used as cyclometalated ligands in heavy metal complexes because of their strong chelating capability and their characteristic optical properties based on π-conjugation. Heavy metal complexes, such as Ir(III) [7, 8] and Pt(II) [9] complexes, have been proven to be excellent phosphorescent dyes for the organic light-emitting diodes (OLEDs).

The electronic structure and optical properties of these heteroatomic conjugated molecules are important factors for developing photofunctional metal complexes. However, simple and strict rules are not applicable for the prediction of the optical properties of polycyclic aromatic hydrocarbons with the possible substitution of heteroatoms, such as N, O, and S. Therefore, theoretical calculations are necessary to understand the relationship between their

Electronic supplementary material The online version of this article (doi:10.1007/s00214-009-0629-6) contains supplementary material, which is available to authorized users.

Y.-P. Lu
Division of Chemistry and Biochemistry, School of Physical and Mathematical Sciences, Nanyang Technological University, 21 Nanyang Link, Singapore 637371, Singapore

M. Ehara (✉)
Institute for Molecular Science, 38 Nishigo-Naka, Myodaiji, Okazaki 444-8585, Japan
e-mail: ehara@ims.ac.jp

M. Ehara
JST-CREST, Sanboncho-5, Chiyoda-ku, Tokyo 102-0075, Japan

molecular structure and optical properties, and to predict the photophysics of these molecules. However, systematic theoretical studies of the excited states of chelating heteroatomic conjugated molecules such as pyridines, benzoxazoles, and benzothiazoles have so far been limited. Only approximate models such as the PPP method or the CNDO method have been applied to these molecules [10]. While these methods are capable of describing the valence-excited states, they are not satisfactory for their accurate prediction. On the other hand, there is increasing use of TD-DFT [11] in calculations of their excited-state properties. Although the TD-DFT calculations provide useful insight into the photophysics and photochemistry of conjugate molecules, the results, in particular the oscillator strength, still need to be validated by other theoretical models.

The SAC (symmetry-adapted cluster) [12]/SAC-CI (SAC-configuration interaction) [13, 14] method has been shown to be reliable and useful for investigating a wide variety of molecular spectroscopic properties in many successful applications [15–17]. This method has been applied to the theoretical spectroscopy of π-conjugated molecules including heteroatomic compounds like furan, pyrrole, and pyridine [16–18]. The optical properties of OLED molecules, such as polyphenylenevinylene (PPV), polyphenylene (PP), and fluorenethiophene (FT) have been examined [19, 20]. Recently, a direct SAC-CI method has been developed [21] and applied to the study of the excited states of π-conjugated molecules like porphin.

In this study, we have systematically investigated the electronic structure and optical properties of 13 conjugate molecules that are widely used for developing iridium (III) complexes, including 2-phenyl pyridine (PPY), 2-phenyl

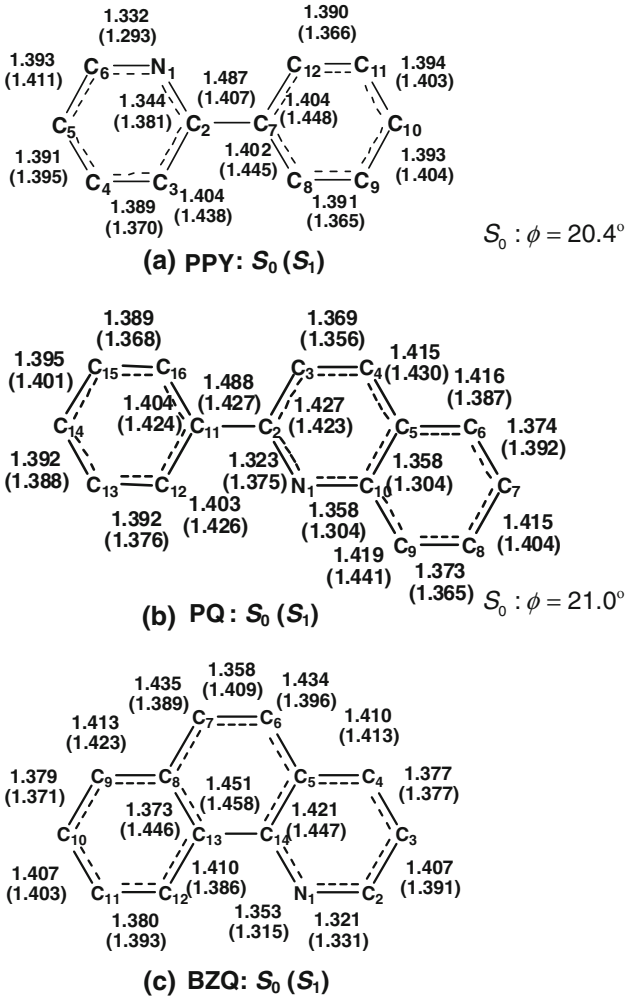

Fig. 1 Equilibrium geometries of PPY, PQ, and BZQ in the S_0 and S_1 states

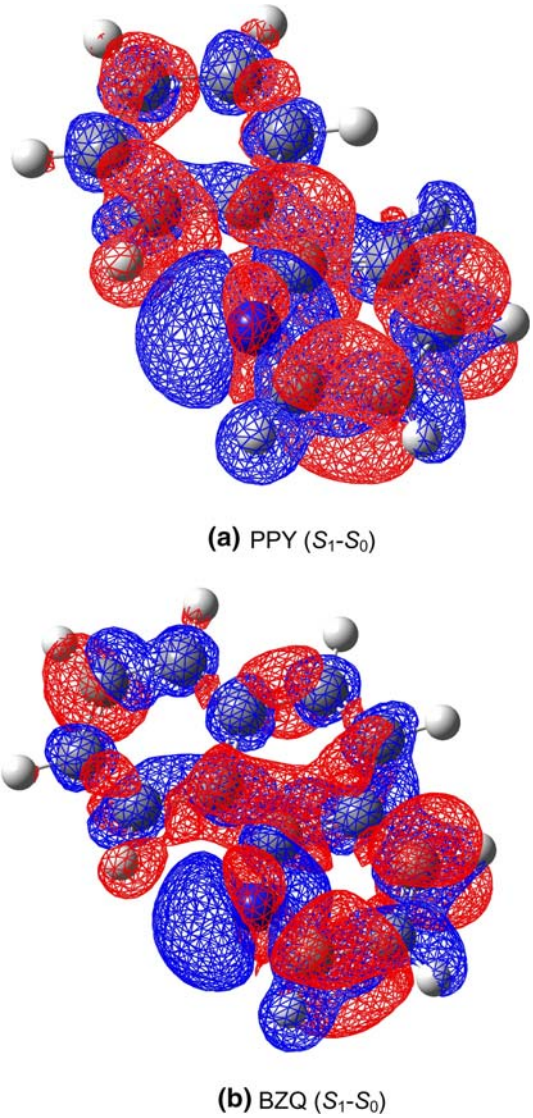

Fig. 2 The SAC-CI electron density difference between the S_0 and S_1 states of **a** PPY and **b** BZQ. The region in the *blue* range has a decrement of electron density and that in the *red* range has an increment of electron density when a molecule is excited

Table 1 Absorption energy, emission energy from the S_1 state, and FIP of PPY, PQ, and BZQ calculated by the SAC-CI method

Molecule	Exptl.[a]	SAC-CI			
	ΔE (eV)	ΔE (eV)	State	Oscillator strength	Transition character
PPY (nonplanar)	Absorption				
	4.49	4.47	*A*	0.015	0.80(H−4 → L) + 0.34(H−4 → L+1)
	5.14	4.49	*A*	0.11	0.57(H → L+1) + 0.44(H → L) − 0.33(H−1 → L)
		4.69	*A*	0.14	0.49(H−1 → L) + 0.47(H → L+2) + 0.46(H → L)
		4.85	*A*	0.001	0.80(H−4 → L+1) − 0.34(H−4 → L)
		5.15	*A*	0.03	0.55(H−2 → L) + 0.43(H → L+2) + 0.33(H−2 → L+1)
		6.33	*A*	0.018	0.53(H → L+1) + 0.53(H−2 → L) + 0.45(H−1 → L)
		6.70	*A*	0.120	0.55(H−3 → L) − 0.41(H−2 → L) − 0.34(H → L+2)
		6.80	*A*	0.15	0.62(H → L+3) − 0.47(H−1 → L+2) + 0.36(H−1 → L+1)
		6.93	*A*	0.32	0.51(H → L+2) + 0.49(H−3 → L) − 0.32(H−1 → L)
		7.09	*A*	0.76	0.54(H−2 → L+1) + 0.41(H−1 → L+1) + 0.37(H−3 → L+1)
	Emission				
		4.18	*A*′	0.55	0.81(H → L) − 0.35(H → L+1)
	FIP				
		7.38	*A*		
PPY (planar)	Absorption				
	4.49	4.54	*A*′	0.11	0.63(H → L+1) + 0.43(H → L) − 0.42(H−1 → L)
	5.14	4.75	*A*′	0.31	0.68(H → L) + 0.44(H−1 → L) + 0.38(H → L+2)
		5.20	*A*′	0.20	0.49(H → L) − 0.47(H → L+1) − 0.38(H → L+2) + 0.33(H−2 → L+1)
		6.40	*A*′	0.03	0.515(H−2 → L) − 0.505(H−1 → L) + 0.48(H → L+1)
		6.74	*A*′	0.19	0.48(H−1 → L+2) − 0.46(H → 1+L + 1) + 0.42(H−3 → L+1) − 0.36(H → L+3)
		4.53	*A*″	0.0026	0.85(H−4 → L)
		5.01	*A*″	0.0011	0.81(H−4 → L+1)
PQ (nonplanar)	Absorption				
	3.87	3.83	*A*	0.099	0.54(H → L) + 0.48(H−1 → L) + 0.43(H → L+1)
	4.35	4.38	*A*	0.029	0.61(H−4 → L) + 0.51(H−5 → L+1)
		4.48	*A*	0.13	0.63(H → L)−0.50(H → L+1)
		4.80	*A*	0.0094	0.54(H−2 → L) + 0.44(H → L+2) + 0.33(H−2 → L+1)
		5.20	*A*	1.10	0.59(H → L+1) + 0.51(H−1 → L+1)
		5.73	*A*	0.053	0.55(H−1 → L+1) − 0.41(H → L+1)
		6.12	*A*	0.094	0.41(H−3 → L) − 0.40(H−1 → L+1) − 0.32(H → L+4)
		6.32	*A*	0.39	0.46(H−3 → L+1) + 0.41(H−1 → L+1)
		6.60	*A*	0.024	0.50(H−3 → L+1) + 0.41(H−2 → L+1)
		6.89	*A*	0.28	0.44(H → L+3) + 0.42(H−2 → L+2)
	Emission				
		3.61	*A*′	0.3	0.67(H → L) − 0.44(H−1 → L) + 0.39(H−1 → L)
	FIP				
		6.89	*A*		
PQ (planar)	Absorption				
	3.87	3.87	*A*′	0.12	0.57(H → L) + 0.46(H−1 → L) − 0.43(H → L+1)
	4.35	4.49	*A*′	0.23	0.69(H → L) − 0.53(H−1 → L) + 0.31(H → L+1)
		4.80	*A*′	0.03	0.55(H−2 → L) + 0.43(H → L+2) + 0.33(H−2 → L+1)
		5.22	*A*′	1.07	0.59(H → L+1) + 0.56(H−1 → L+1)
		5.76	*A*′	0.10	0.70(H−1 → L+1) + 0.40(H → L+1)
		3.75	*A*″	0.0020	0.90(H−4 → L)
		4.76	*A*″	0.0001	0.89(H−4 → L+1)

Table 1 continued

Molecule	Exptl.[a]	SAC-CI			
	ΔE (eV)	ΔE (eV)	State	Oscillator strength	Transition character
BZQ	Absorption				
	3.57	3.70	A'	0.02	0.66(H → L) − 0.48(H−1 → L+1)
	4.63	4.54	A'	0.03	0.58(H → L+1) + 0.57(H−1 → L) − 0.37(H → L)
		4.82	A'	0.31	0.44(H−1 → L+2) + 0.33(H → L) − 0.31(H−2 → L)
		5.14	A'	0.21	0.52(H → L+1) − 0.43(H−1 → L) + 0.39(H−1 → L+1)
		5.42	A'	0.77	0.45(H−1 → L) + 0.45(H−1 → L+1) + 0.42(H−2 → L)
		4.12	A''	0.0026	0.85(H−4 → L)
		4.67	A''	0.0001	0.86(H−4 → L+1)
		6.26	A''	0.0006	0.79(H−4 → L+2)
		7.00	A''	0.0015	0.87(H−6 → L+1)
	Emission				
	3.53	3.57	A'	0.03	0.59(H → L+1) − 0.49(H−1 → L) − 0.44(H → L)
	FIP				
		7.29	A''		

PPY 2-phenyl pyridine, *PQ* 2-phenyl quinoline, *BZQ* benzo[h]quinoline

[a] From [32–34]

quinoline (PQ), bonzo[h]quinoline (BZQ), 2,5-diphenyl-oxazole (DPO), 2-phenyl-benzoxazole (BO), 1-(1-naphthyl)-benzoxazole (BON), 2-phenyl-oxazoline (OP), 2-phenyl-benzothiazole (BT), 2-(2-benzothienyl)-pyridine (BTP), 2-(1-naphthyl)-benzothiazole (αBSN), 2-(2-naphthyl)-benzothiazole (βBSN), 2-(2-thienyl)-pyridine (THP), and 2-(2-thienyl)-benzothiazole (BTTH), by SAC-CI method. The present calculations provide useful information regarding the energy levels of chelating heteroatomic conjugated compounds for the development of luminescent metal complexes including their fine color tuning, and also as a basis for the further theoretical study of their optical properties.

2 Computational details

We have calculated the electronic structure and optical properties of 13 chelating heteroatomic conjugated molecules. The ground-state geometries of the molecules were optimized by using the B3LYP [22–24]/6–311G(d) [25, 26] method and these theoretically optimized structures were used for calculations of their vertical excitation energy. To calculate their fluorescence emission energy, the geometries in the first singlet excited state of these compounds were optimized with the CIS [27]/6–311G(d) method. It was confirmed that all the equilibrium structures are at true local minima by vibrational analysis. The results of the vibrational analysis for all the molecules were compiled in the supporting data.

The absorption and emission energies were calculated using the SAC/SAC-CI singles and doubles (SD)–*R* method by directly calculating the σ-vector in a direct SAC-CI approach [21]. The basis sets of the SAC-CI calculations are the double-zeta plus one polarization functions (DZP) of Huzinaga–Dunning for the C, N, O, S, and H atoms [28]. We focus on the valence-excited states that are relevant for the optical properties of photofunctional molecules. We also examined the effect of Rydberg p functions on each first- or second-row atom. The perturbation selection technique was adopted to reduce the computational cost, and LevelTwo accuracy was used. The threshold of the linked terms for the ground state was set to $\lambda_g = 5.0 \times 10^{-6}$. All the product terms generated by doubles were included in the SAC calculation. For the excited and ionized states, the thresholds of the linked doubles were set to $\lambda_e = 5.0 \times 10^{-7}$. All the product terms generated by the R_1S_2 and R_2S_2 operators were included in the SAC-CI calculations.

The SAC/SAC-CI calculations were performed with the Gaussian03 suite of programs [29] with modifications for executing the direct SAC-CI method [21].

3 Results and discussion

To facilitate the discussion, we have categorized the molecules into three groups: (I) PPY, PQ, and BZQ; (II) DPO, BO, BON, and OP; and (III) BT BTP, αBSN, βBSN THP,

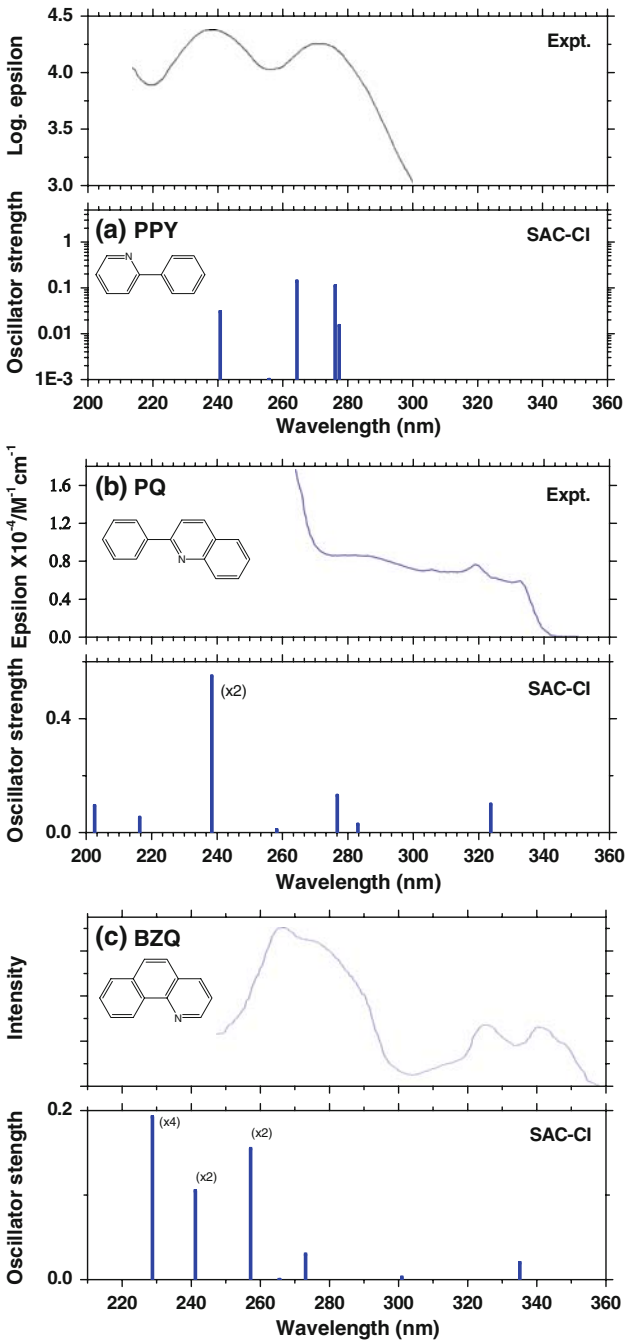

Fig. 3 Theoretical absorption spectra of **a** PPY, **b** PQ, and **c** BZQ compared with the experimental spectra. Experimental spectra are cited from [32–34]

and BTTH, based on the type and number of heteroatoms in their molecular structures.

3.1 Group I: PPY, PQ, and BZQ

Each compound in this group contains one N atom in the conjugated ring. Figure 1 illustrates the calculated geometries of these compounds in the ground state (S_0) and the lowest $\pi\pi^*$ excited state (S_1) with the CC bond lengths. In the S_0 state of PPY, a nonplanar structure is most stable with the torsion angle of 20.4° (dihedral angle of $N_1C_2C_7C_{12}$); the energy difference between planar and nonplanar structure is about 0.19 kcal/mol. PQ also has a local minimum at nonplanar structure with the dihedral angle of $N_1C_2C_{11}C_{12}$ being 21.0°. As a fused ring molecule, BZQ is planar in the S_0 state. These three molecules were calculated to be planar in the lowest $\pi\pi^*$ excited state. Therefore, PPY becomes planar from a nonplanar structure by the S_0–S_1 excitation. The inter-ring CC bond distance is 1.488 Å in S_0 and the bond shrinks significantly to 1.407 Å in S_1, the change of bond length amounting to 0.081 Å. The bonds in the pyridyl and phenyl rings also become elongated or shortened alternatively by the S_0–S_1 excitation, but the bond angles CCH and CCC do not change as much. The same trends can be observed in PQ: it becomes planar in S_1 and the inter-ring CC bond becomes significantly shortened from 1.491 Å in S_0 to 1.427 Å in S_1, and the other bonds in the rings change alternatively. Again, we did not find a large change in bond angles for PQ. Finally, when BZQ is excited to an S_1 state, bonds in this fused ring molecule become shortened or elongated, but there is no dominant bond distance change in a single pair of atoms, as the geometry relaxation spreads out almost evenly over the entire molecule.

The geometry relaxation in the excited state can be interpreted using the electrostatic force (ESF) theory [30, 31]. As an example, we discuss the geometric changes in the S_1 state of PPY and BZQ. In ESF theory, geometry relaxation in the excited state is due to the force acting on nuclei caused by changes in electron distribution. The Coulombic force exerted on the nuclei induces movements of the nuclei to accompany the change in the electron distribution until the forces diminish at the excited-state geometry. The molecular shape in the ground and excited states is determined by balancing of the atomic dipole (AD), exchange (EC), and gross charge (GC) forces. The differences in the SAC-CI electron density between the S_0 and S_1 states in PPY and BZQ are shown in Fig. 2. In PPY, the electron density in the C–C (C_2–C_3, C_7–C_{12}, C_7–C_8) and C_2=N_1 bonds in the phenyl ring and pyridyl ring decrease, while the density of the inter-ring C_2–C_7 bond significantly increases and there are some increments in the intra-ring C–C (C_3–C_4, C_8–C_9, C_{11}–C_{12}) and C_6–N_1 bonds. The EC force along bonds including the C_2=N_1 and C_2–C_3 bonds decreases because of the decrement of electron density, whereas the EC force is enhanced along the C_2–C_7, C_6–N_1, and C_3–C_4 bonds. Consequently, the former bond lengths increase, and the latter bond lengths decrease. This geometry change enhances the conjugation between two rings and the S_1 structure of PPY becomes planar. In BZQ, the

Table 2 Absorption energy, emission energy from the S_1 state, and FIP of DPO, BO, BON, and OP calculated by the SAC-CI method

Molecule	Exptl.[a]	SAC-CI			
	ΔE (eV)	ΔE (eV)	State	Oscillator strength	Transition character
DPO	Absorption				
	4.09	4.14	A'	0.88	0.92(H → L)
	5.49	4.72	A'	0.013	0.40(H → L+2) − 0.40(H → L+3) + 0.35(H → L+1)
		4.79	A'	0.0034	0.42(H−1 → L) + 0.38(H → L+2) + 0.35(H−2 → L)
		5.63	A'	0.050	0.73(H → L+1)
		5.55	A''	0.0024	0.85(H−6 → L)
	Emission				
	3.40	3.42	A'	0.72	0.82(H → L)
	FIP				
		6.50	A''		
BO	Absorption				
	4.05	4.52	A'	0.48	0.69(H → L)
		4.73	A'	0.0073	0.66(H−2 → L) − 0.44(H → L+1) + 0.37(H−3 → L+1)
		5.03	A'	0.32	0.49(H → L) + 0.45(H−1 → L) − 0.43(H → L+3)
		6.12	A'	0.082	0.57(H−1 → L) + 0.55(H → L+2)
		6.51	A'	0.012	0.79(H−3 → L) − 0.35(H−2 → L+1)
		5.26	A''	0.0029	0.87(H−4 → L)
	Emission				
	3.62	3.80	A'	0.79	0.88(H → L)
	FIP				
		7.11	A''		
BON	Absorption				
	3.44	3.85	A'	0.55	0.89(H → L)
		4.01	A'	0.024	0.67(H−2 → L) − 0.52(H → L)
		4.75	A'	0.012	0.45(H−3 → L) − 0.39(H−1 → L) + 0.35(H−3 → L+2)
		5.12	A'	0.14	0.75(H−1 → L)
		6.19	A'	0.14	0.54(H−3 → L) + 0.38(H → L+3) + 0.37(H−1 → L+2)
		4.95	A''	0.0022	0.85(H−5 → L)
	Emission				
	3.44	3.36	A'	0.60	0.90(H → L)
	FIP				
		6.55	A''		
OP	Absorption				
		4.67	A	0.0025	0.68(H−1 → L) − 0.59(H → L+1)
		5.20	A	0.25	0.67(H → L)
		5.43	A	0.0051	0.85(H−3 → L) + 0.38(H−3 → L+3)
		6.27	A	0.056	0.76(H−2 → L) − 0.35(H → L) − 0.33(H−1 → L+1)
		6.86	A	0.55	0.71(H → L+1) + 0.60(H−1 → L)
		7.16	A	0.79	0.87(H−1 → L+1)
	Emission				
		4.47	A	0.10	0.56(H−1 → L) + 0.49(H → L) − 0.48(H → L)
		4.57	A	0.23	0.67(H → L) + 0.38(H−1 → L) + 0.37(H → L)
	FIP				
		7.81	A		

DPO 2,5-diphenyl-oxazole, *BO* 2-phenyl-benzoxazole, *BON* 2-(1-naphthyl)-benzoxazole, *OP* 2-phenyl-oxazoline

[a] From [34–36]

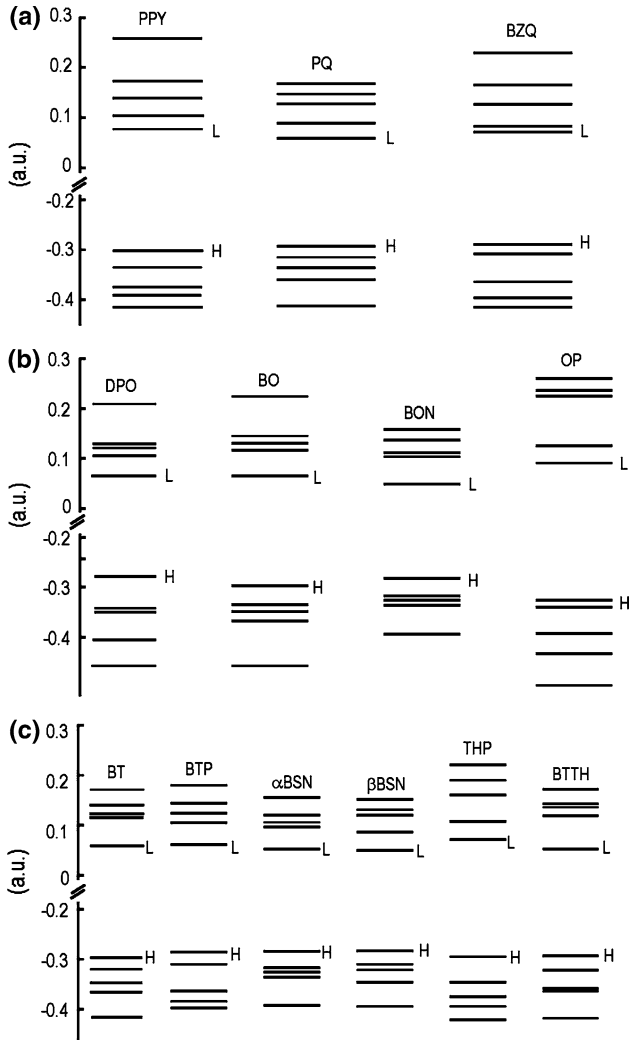

Fig. 4 Orbital energy level diagrams of the heteroatomic conjugated molecules in **a** Group I, **b** Group II, and **c** Group III

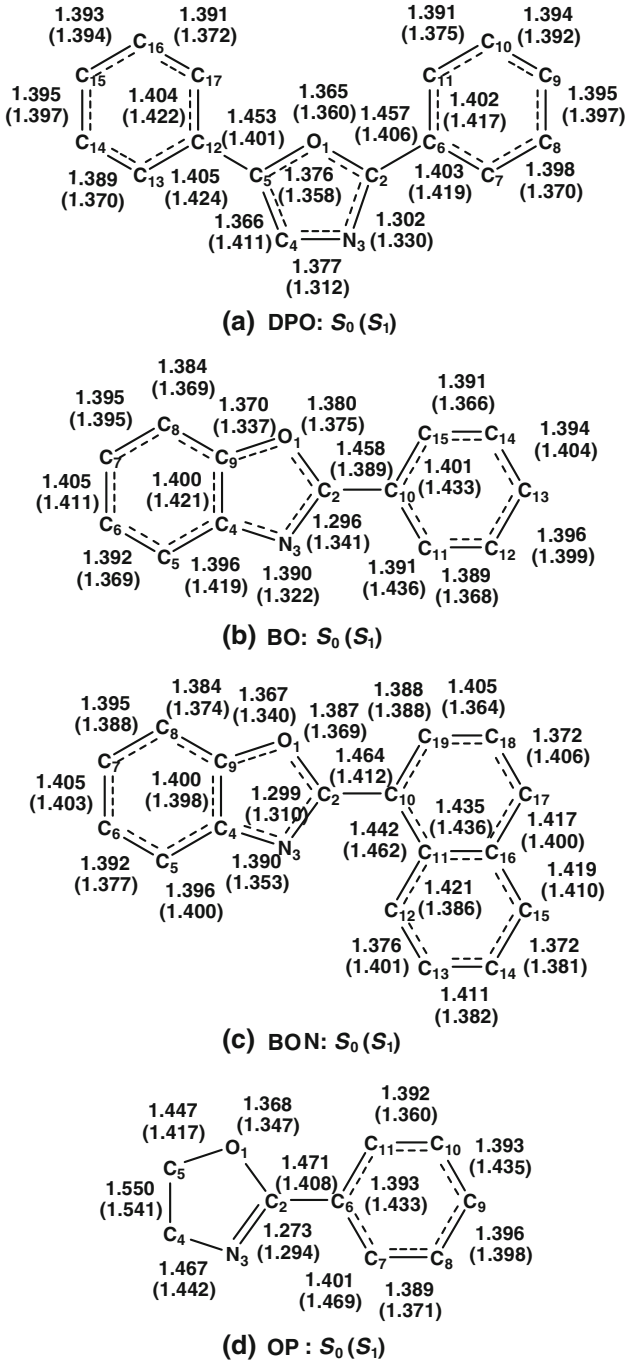

Fig. 5 Equilibrium geometries of DPO, BO, BON, and OP in the S_0 and S_1 states

electron density increases and decreases alternatively in small magnitudes over the entire molecule.

Next, we discuss the absorption and emission spectra of these molecules. Table 1 shows the vertical excitation energies and oscillator strengths obtained by using the SAC-CI method with the available experimental values. For the absorption spectra, we have listed the results for both the nonplanar and planar PPY and PQ. These molecules are important ligands to form the heavy metal complexes and they all have planar geometries in the complexes. Therefore, the absorption spectra and energy levels at the planar geometries are of interest for PQ and PPY, and we calculated the spectra at planar geometries which were obtained by restricting the C_s structure. Also the energy difference between the planar and nonplanar structures is only 0.19 kcal/mol for both molecules, so that the conformer of the wide range of torsion angle contributes to the excitation spectra at room temperature. The emission energy from the lowest $\pi\pi^*$ excited state and the first ionization potential (FIP) are also listed in the same table. In the heteroatomic conjugated molecules, the $\pi\pi^*$ and $n\pi^*$ excitations exist. In the nonplanar PPY and PQ, both excitations are labeled as A state in C_1 symmetry, and in the planar PPY, PQ, and BZQ, the $\pi\pi^*$ and $n\pi^*$ excitations are labeled as the A' and A'' states, respectively, in C_s symmetry. The $\pi\pi^*$ transitions may have large oscillator

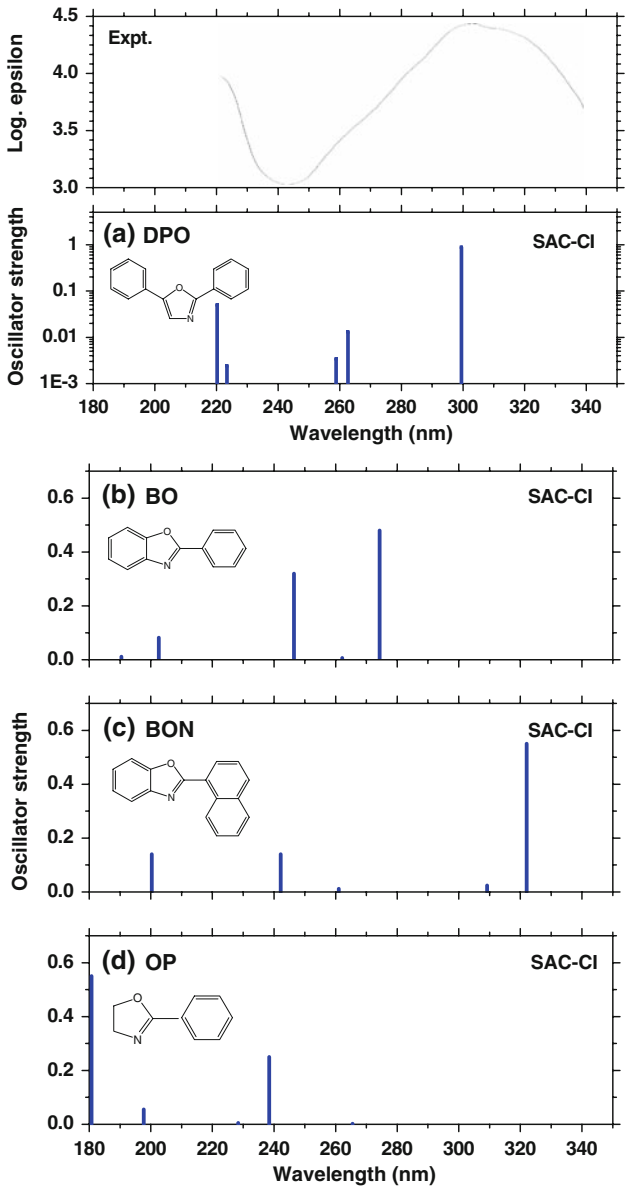

Fig. 6 Theoretical absorption spectra of **a** DPO, **b** BO, **c** BON, and **d** OP. Experimental spectrum of DPO is cited from [35]

strengths, while the $n\pi^*$ transitions have small oscillator strengths. The experimental and theoretical absorption spectra of these molecules are compared in Fig. 4. The calculated spectra satisfactorily reproduced the position of the observed absorption peaks for PPY and PQ, and an accuracy of 0.3 eV was achieved in the calculation result of BZQ. As noted in Sect. 2, we focus on the valence-excited states in this work. We examined the effect of the diffuse Rydberg p-type AOs placed on each C and N atom; however, the effect was small for all the valence-excited states. For example, by including Rydberg p-type AOs, the first absorption peak was red-shifted by 0.09 eV for PPY, 0.18 eV for PO, and 0.20 eV for BZQ. Therefore, we present the results with the DZP basis sets for all the molecules.

Based on the SAC-CI calculations for PPY at the nonplanar structure, we assign the broad peak around 4.49 eV (276 nm) [32] as the second and third transitions calculated as 4.49 and 4.69 eV. These transitions are characterized as the HOMO–LUMO+1 (H–L+1) and HOMO–LUMO (H–L) transitions, respectively. The oscillator strength in each transition is relatively large, 0.11 and 0.14, respectively. Thus, the peak around 5.14 eV (242 nm) [32] is assigned as the transition with a vertical excitation energy of 5.15 eV. These transitions are mainly due to $\pi\pi^*$ transitions. The first and fourth transitions calculated as 4.47 and 4.85 eV also account for the broad peak around 4.49 eV [32], although their oscillator strength is much smaller than the second and third transitions. These two transitions belong to $n\pi^*$ transitions. Below the ionization threshold calculated as 7.38 eV, there are four strong higher excited states in the range from 6.7 to 7.1 eV. The emission energy for the S_1–S_0 transition calculated at the S_1 state geometry is 4.18 eV. No experimental observation was reported for this fluorescence. The absorption energy spectrum of the planar structure is similar to that of the nonplanar one, which indicates that the thermal effect on the absorption spectrum is not so large.

The SAC-CI calculation for PQ shows that the strongest transition occurs at an energy of 5.22 eV with an oscillator strength of 1.07. The experimental spectrum gives a strong indication that the absorption is very strong above 4.76 eV (260 nm) [33], although no experimental value has been reported. The absorption energies of 3.87 and 4.49 eV in our calculations are consistent with the structures at 3.87 eV (320 nm) and 4.35 eV (285 nm) in the experimental absorption spectra [33] as shown in Fig. 3 and there is also a minor peak at 4.38 eV, which belongs to $n\pi^*$ transitions. The structure relaxation in the excited state causes the fluorescence emission at 3.61 eV. The calculated FIP is 6.89 eV. As in the case of PPY, our calculations show that the absorption spectrum of the planar PQ is very close to that in the nonplanar one.

For the strong asymmetric absorption peak of BZQ observed at 4.64 eV (267 nm) [34], we obtained the excited states at 4.52 eV (274 nm) and 4.82 eV (257 nm). The former state corresponds to the shoulder in the lower energy region, while the latter contributes to the main absorption, with a large oscillator strength of 0.31. We also calculated the state at 3.70 eV with a non-negligible oscillator strength of 0.02. This matches with the side band at around 3.75 eV (330 nm) in the experimental absorption spectrum [34]. The calculated fluorescence emission energy was 3.57 eV, which was in excellent agreement with the observed value of 3.53 eV (351 nm) [34]. The SAC-CI results for BZQ are in good agreement with the

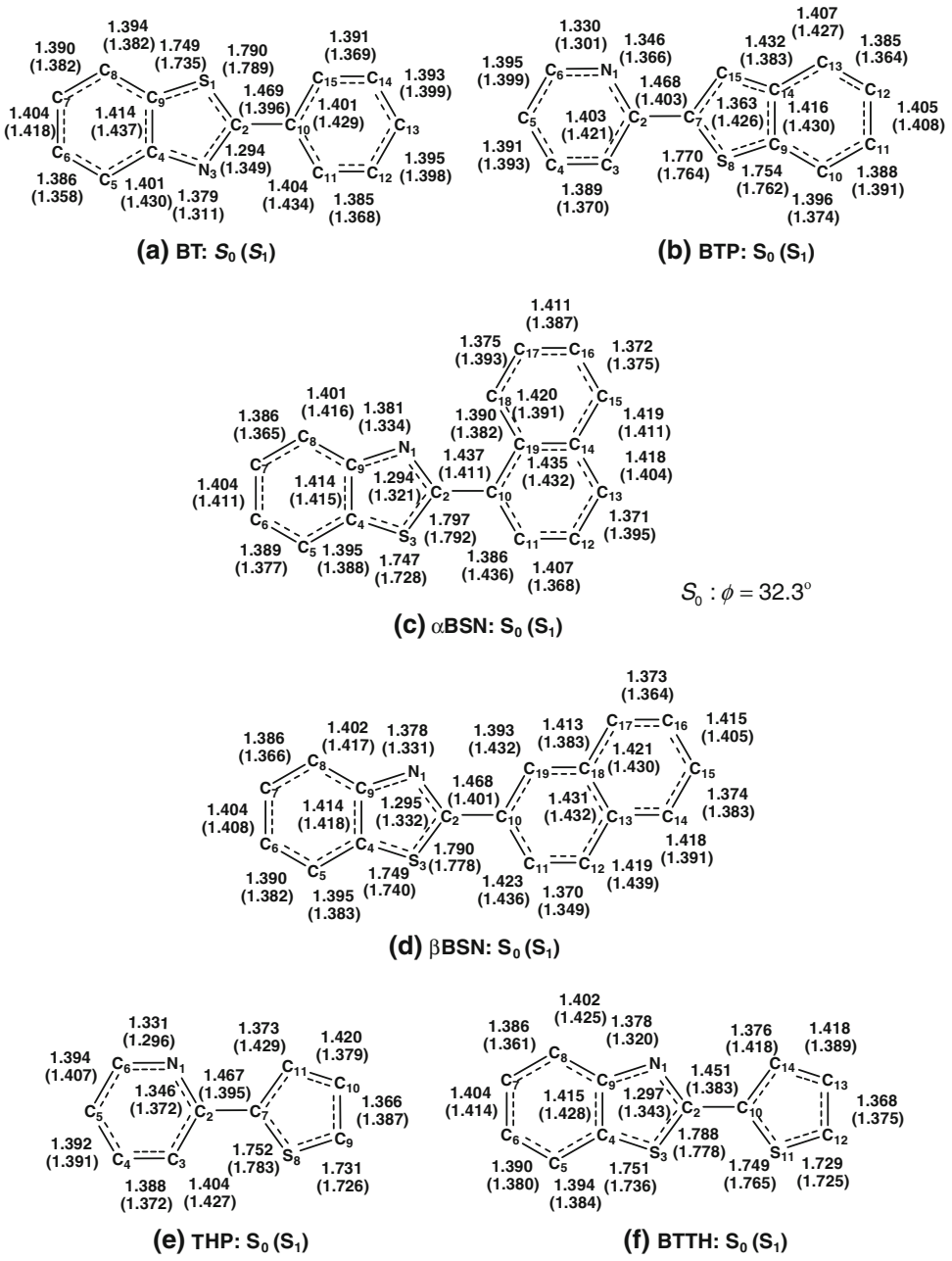

Fig. 7 Equilibrium geometries of BT, BTP, αBSN, βBSN, THP, and BTTH in the S_0 and S_1 states

available experimental data. The FIP was calculated to be 7.29 eV, which is close to the value for PPY.

The transition character in Table 2 shows that there are mixed contributions from H–L transitions and the transitions among HOMO−2 and HOMO−1 to LUMO+1 and LUMO+2. In these conjugate molecules, MOs from HOMO − 2, to LUMO+2 belong to the π/π^* orbitals. We have plotted the orbital energy for these pyridine derivatives in Fig. 4a. The orbital energy diagram reveals that the energy gap between HOMO and the next HOMO in each compound is small, as is that of LUMO and the next LUMO, in particular for BZQ.

According to the simple one-dimensional model, if the first absorption peaks were assumed to be transitions from HOMO to LUMO in these conjugate molecules, the approximate conjugate lengths were calculated to be 2.6 Å for PPY, 3.1 Å for BZQ, and 3.2 Å for PQ. These estimated effective conjugated lengths are consistent with the size of these conjugate molecules.

3.2 Group II: DPO, BO, BON, and OP

The compounds in this group contain oxygen and nitrogen atoms in their conjugated rings. The optimized structures

Table 3 Absorption energy, emission energy from the S_1 state, and FIP of BT, BTP, αBSN, βBSN, THP, and BTTH calculated by the SAC-CI method

Molecule	SAC-CI			
	ΔE (eV)	State	Oscillator strength	Transition character
BT	Absorption			
	4.25	A'	0.18	0.57(H−1 → L) − 0.49(H → L)
	4.51	A'	0.53	0.75(H → L) − 0.44(H−1 → L)
	4.69	A'	0.059	0.65(H−2 → L) − 0.35(H → L+2)
	5.53	A'	0.086	0.47(H → L+2) − 0.47(H−1 → L) − 0.39(H → L+1)
	6.21	A'	0.22	0.61(H−3 → L) − 0.43(H−1 → L+2)
	4.56	A''	0.001	0.89(H−5 → L)
	6.07	A''	0.0006	0.68(H−1 → L+4) − 0.56(H → L+4)
	Emission			
	3.64	A'	0.76	0.90(H → L)
	FIP			
	7.05	A''		
BTP	Absorption			
	4.10	A'	0.16	0.75(H−1 → L)
	4.15	A'	0.57	0.87(H → L)
	4.76	A'	0.083	0.64(H → L+1)
	5.33	A'	0.11	0.67(H → L+2)
	5.95	A'	0.18	0.78(H−1 → L+2)
	4.40	A''	0.0026	0.80(H−5 → L)
	4.86	A''	0.0013	0.81(H−5 → L+1)
	Emission			
	3.63	A'	0.82	0.91(H → L)
	FIP			
	6.69	A''		
αBSN	Absorption			
	4.00	A	0.45	0.87(H → L)
	4.11	A	0.03	0.54(H → L+1) + 0.54(H−3 → L)
	4.49	A	0.05	0.55(H−1 → L) + 0.38(H−1 → L+2)
	5.02	A	0.03	0.77(H−6 → L)
	5.20	A	0.13	0.61(H−2 → L) − 0.36(H−1 → L) + 0.33(H−3 → L)
	Emission			
	3.25	A'	0.56	0.87(H → L)
	FIP			
	6.48	A		
βBSN	Absorption			
	3.80	A'	0.091	0.55(H−1 → L) − 0.47(H → L) − 0.44(H → L+1)
	4.03	A'	0.62	0.74(H → L)
	4.45	A'	0.024	0.60(H−2 → L) + 0.34(H−2 → L+3) + 0.33(H → L+2)
	4.96	A'	0.66	0.64(H → L+1) + 0.51(H−1 → L)
	5.63	A'	0.14	0.51(H−2 → L) − 0.44(H → L+2) − 0.31(H−2 → L+2)
	4.62	A''	0.0009	0.84(H−6 → L)
	5.84	A''	0.0001	0.77(H−1 → L+5) + 0.42(H−1 → L+5)
	6.04	A''	0.0004	0.85(H−2 → L+5)
	Emission			
	3.42	A'	0.84	0.89(H → L)
	FIP			
	6.53	A''		

Table 3 continued

Molecule	SAC-CI			
	ΔE (eV)	State	Oscillator strength	Transition character
THP	Absorption			
	4.34	A'	0.36	0.77(H → L) − 0.40(H → L+1)
	4.77	A'	0.19	0.65(H → L+1) + 0.49(H → L) + 0.37(H−2 → L)
	5.21	A'	0.11	0.82(H−1 → L)
	6.16	A'	0.014	0.65(H−2 → L) − 0.46(H → L+1)
	6.71	A'	0.095	0.78(H → L+2)
	4.52	A''	0.0029	0.80(H−4 → L) − 0.43(H−4 → L+1)
	5.01	A''	0.001	0.81(H−4 → L+1)
	6.29	A''	0.0001	0.88(H → L+3)
	6.56	A''	0.0002	0.92(H−1 → L+3)
	Emission			
	3.83	A'	0.52	0.88(H → L)
	FIP			
	7.20	A''		
BTTH	Absorption			
	3.98	A'	0.52	0.81(H → L)
	4.32	A'	0.20	0.66(H−1 → L) − 0.40(H → L)
	5.06	A'	0.056	0.79(H−2 → L)
	5.45	A'	0.15	0.57(H → L+1) − 0.44(H−1 → L)
	5.88	A'	0.076	0.83(H−3 → L)
	4.67	A''	0.0011	0.88(H−5 → L)
	5.19	A''	0.0002	0.9(H → L+3)
	5.76	A''	0.0005	0.81(H−1 → L+3)
	Emission			
	3.40	A'	0.71	0.90(H → L)
	FIP			
	6.92	A''		

BT 2-phenyl-benzothiazole, *BTP* 2-(2-benzothienyl)-pyridine, *αBSN* 2-(1-naphthyl)-benzothiazole, *βBSN* 2-(2-naphthyl)-benzothiazole, *THP* 2-(2-thienyl)-pyridine, *BTTH* 2-(2-thienyl)-benzothiazole

for these compounds in both the S_0 and S_1 states are shown in Fig. 5. Except for OP, all the molecules in this group have a planar structure in both their S_0 and S_1 states. OP has two sp^3 carbons, which causes a nonplanar structure. Because the molecular structures for these compounds consists of two conjugate rings connected by a single bond and the HOMO and LUMO have antibonding and bonding characters, respectively, in this bond, one can expect that there is a large geometry change for this single bond in the S_0–S_1 transition. In DPO, the C_2–C_6 distance is 1.457 Å in S_0 and 1.406 Å in S_1, and the C_5–C_{12} distance is 1.453 Å in S_0 and 1.401 Å in S_1; both single bonds shrink by about 0.05 Å. There is also large geometry relaxation in the central ring; that is, the C_4–C_5 and C_4–N_3 distances change from 1.366 to 1.411 Å and from 1.377 to 1.312 Å, respectively. In BO, the central link bond C_2–C_{10} changes from 1.458 Å in S_0 to 1.389 Å in S_1. The ring structure also changes, in particular the bonds connected to the C_2 and C_{10} atoms; bond length changes are C_2–N_3 = +0.045 Å, C_{10}–C_{11} = +0.035 Å, and C_{10}–C_{15} = +0.033 Å. In BON, the C_2–C_{10} bond distance also changes from 1.464 to 1.412 Å in the S_0–S_1 transition. The five-membered ring connected to this single bond also deforms from the excitation because the excitation is relatively localized in the central part of the molecule. In OP, the central C_2–C_6 bond length changes from 1.471 to 1.408 Å when OP changes its electronic state. Such geometry relaxation arises from the changes in the electron distribution between the ground and excited states as was discussed for the aforementioned molecules.

In Table 2, we summarize the SAC-CI results for the vertical absorption energies, oscillator strength, vertical emission energy of the S_1–S_0 transition, and FIP for these four molecules. Theoretical spectra for these molecules are shown in Fig. 6. DPO is a common fluorescent laser dye with high quantum efficiency in the UV/violet fluorescence at room temperature [35]. The SAC-CI calculation satisfactorily reproduced the main peak; the calculated value is

4.14 eV, which is in excellent agreement with the experimental spectrum peaking at 4.09 eV. Comparison is also made between the theoretical and experimental spectra in Fig. 6a. This excitation is dominantly described by the H–L transition with significantly large oscillator strength of 0.88. The calculations also reproduced the position of the shoulder at around 260 nm (4.76 eV) and the second peak at around 226 nm (5.49 eV) observed in the experimental work [35]. For the emission energy, the calculated value is 3.42 eV based on the S_1 structure, and the experimental emission spectrum has a peak at 3.40 eV [35]. The FIP was estimated as 6.50 eV.

The BO and BON molecules belong to the benzoxazole derivatives. We have calculated the first absorption peaks for BO at 4.52 eV, which is about 0.47 eV higher than the experimental value [36]. For BON, the SAC-CI calculations also gave a higher value for the first absorption peak of 3.85 eV compared with the experimental value of 3.44 eV [36]. We note that these experimental spectra are measured with low resolution. The absorption energy of BO is higher than that for BON, reflecting the effective conjugate length. For the emissions of these molecules, we report the transition energies as 3.83 eV for BO and 3.36 eV for BON. Both values show good agreement with the respective experimental data of 3.62 and 3.44 eV [36]. The FIP was obtained as 7.11 eV for BO and 6.55 eV for BON by the SAC-CI calculation.

Compared with other compounds in this study, the effective conjugation length of OP is the shortest because the five-membered ring is not a fully conjugated group. The theoretical results reflect this. The absorption peak with a large oscillator strength lies at 5.20 eV, and all the other excited states are also located in a relatively high-energy range in the UV region. The local minimum of S_1 could not be obtained for OP, since two different excited states lie close in energy. We calculated the emission energies for the $S_1 \rightarrow S_0$ transition as 4.47 and 4.57 eV at the optimized structures restricted in C_s. The FIP is 7.81 eV.

The orbital energy diagrams for these four compounds are compared in Fig. 4b. The first absorption peaks for DPO, BO, and BON are mainly characterized as the H–L transition. In DPO, the energy gap between HOMO and next HOMO orbitals is large, and in BO and BON, the energy gap between LUMO and next LUMO orbitals is large. The energy gaps of H–H−1 and L–L+1 of OP are small, and the lowest excited state of OP is characterized as H−1 → L and H → L−1.

3.3 Group III: BT, BTP, αBSN, βBSN, THP, and BTTH

The compounds in this group contain sulfur and nitrogen atoms and belong to the group of benzothiazole derivatives, except for BTP and THP, which are pyridine derivatives. BT/BTP and αBSN/βBSN are two pairs of isomers. Figure 7 shows the optimized geometries of these compounds in their S_0 and S_1 states. The most striking observation occurs for αBSN. Unlike the other molecules in this group, it has a nonplanar structure in its S_0 state. The torsion angle between the benzothiazole ring and the naphthalene ring is 32.33° (dihedral angle of $N_1C_2C_{10}C_{19}$). However, in its S_1 state, it becomes planar as the inter-ring C–C single bond has a higher bond order, as evidenced by the C_2–C_{10} distance change from 1.437 Å in S_0 to 1.411 Å in S_1. The geometry relaxations in the S_1 state of other molecules in this group show a similar scenario to PPY.

Table 3 shows the absorption energies, oscillator strengths, and emission energies from the S_1 state, and the FIP. Theoretical spectra of these molecules are displayed in Fig. 8. Unfortunately, to the best of our knowledge, there are no experimental data for these molecules and therefore

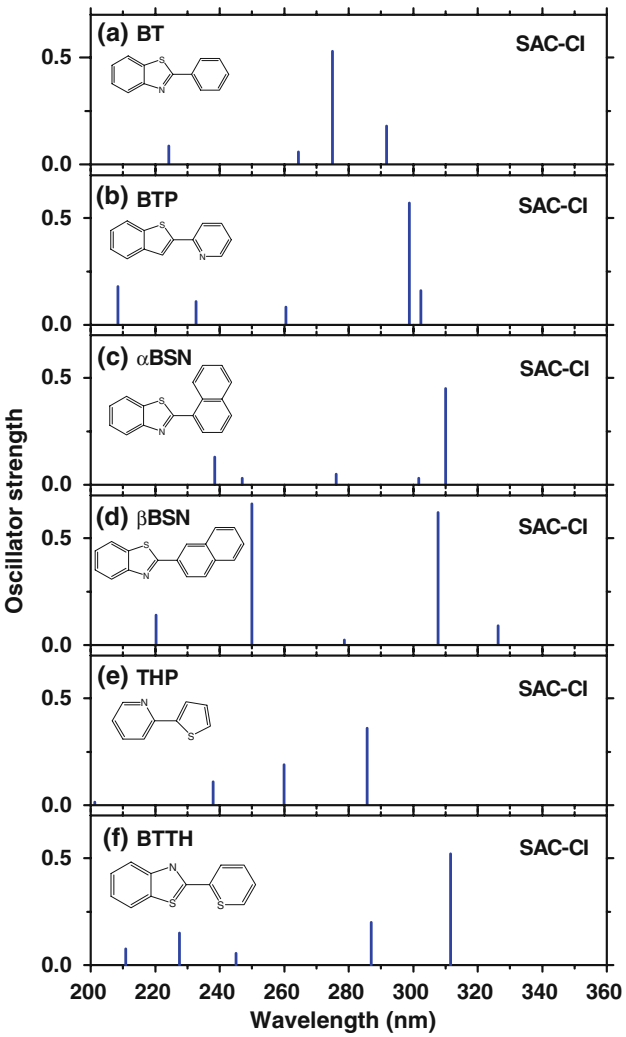

Fig. 8 Theoretical absorption spectra of **a** BT, **b** BTP, **c** αBSN, **d** βBSN, **e** THP, and **f** BTTH

to understand how the π-conjugated structure in isomers influences the absorption and emission properties in conjugate molecules, our attention is focused on the two pairs of isomers.

The first peak of BT is located at 4.25 eV and the second at 4.51 eV. For both transitions, the oscillator strength is large, 0.18 and 0.53, respectively. Because the transition dipole is large for the H–L transition and the transition at 4.51 eV has a larger H–L component than the transition at 4.25 eV, the oscillator strength of the second peak is stronger. For BTP, we also found that the oscillator strength of the second peak at 4.15 eV (0.57) is larger than the first peak at 4.10 eV (0.16). Again, the H–L transition is the dominant component in the second peak. The change from the phenyl ring to a pyridyl ring causes a reduction of the H–L and H–1−L energy gaps so that the first and second peaks of BTP are lower in energy than BT, but the calculated emission energies are not so different between these molecules.

The second isomer pair, αBSN and βBSN, is stereoisomers. As we have mentioned, αBSN is a nonplanar molecule in the ground state, but the structure of βBSN is planar. In our calculations, the first peak of absorption for αBSN is located at 4.00 eV, while that for βBSN is at 3.81 eV. This reflects the fact that βBSN has a longer conjugate length than αBSN. The first peak in αBSN is mainly due to the H–L transition, but that of βBSN has contributions from the H–L transition as well as the transition from/to the next HOMO and the next LUMO.

The results for the other two compounds in this group, THP and BTTH, are listed in Table 3. The lowest peaks are characterized as the H–L transitions and have large oscillator strength. We also plot the orbital energy diagram for this group in Fig. 6c. The energy separations of H–H−1 and L–L+1 are large for THP and BTTH.

4 Summary

We have investigated the electronic structure and optical properties of 13 chelating heteroatomic conjugated molecules such as pyridine, benzoxazole, and benzothiazole derivatives, which are used as C–N ligands in organometallic compounds by using the SAC-CI method. The local minima of the ground- and first-excited-state geometries were located and confirmed by the vibrational analysis using the DFT and CIS methods, respectively. Four molecules, PPY, PQ, αBSN, and OP, are nonplanar in their ground state, but all the molecules except for OP have planar geometries in the lowest $\pi\pi^*$ excited state. Other molecules were calculated to be planar in their ground states. The SAC-CI calculations of the absorption and emission energies were applied to these molecules at the optimized geometry.

For the six compounds whose experimental data are available, the SAC-CI calculations reproduced the experimental values satisfactorily with deviations of less than 0.3 eV for absorption and 0.1 eV for emission, except for BO and BON. For other molecules, the theoretical absorption and emission spectra were predicted. The S_0 and S_1 geometries were calculated to be planar for all the molecules except for βBSN. The geometry change due to the S_0–S_1 transition was qualitatively interpreted using the ESF theory based on the SAC/SAC-CI electron density difference. The excitations are localized in the central region of the molecules and in the S_1 state; the inter-ring single bond shows a large change with a contraction of 0.05–0.09 Å.

The present SAC-CI calculations provide useful information regarding the energy levels of chelating heteroatomic conjugated compounds for developing luminescent metal complexes for fine color tuning, and also provide the basis for the further theoretical study of the optical properties of metal complexes.

Acknowledgments The authors would like to thank Dr. R. Fukuda and Prof. H. Nakatsuji for the direct SAC-CI program code. They also thank the reviewers for the valuable comments. This study was supported by the JSPS Exchange Program for East Asian Young Researchers. M.E. was supported by the grant from the JST-CREST, Scientific Research in Priority Areas "Molecular Theory for Real Systems" from the Ministry of Education, Culture, Sports, Science and Technology of Japan, the Next Generation Supercomputing Project, and the Molecular-Based New Computational Science Program, NINS. A part of the computations were performed at Research Center for Computational Science, Okazaki, Japan.

References

1. Kalle C (1962) Brirtish Patent 895001
2. Mori A, Sekiguchi A, Masui K, Shimada T, Horie M, Osakada K, Kawamoto M, Ikeda T (2003) J Am Chem Soc 102:1700
3. Williams DL, Heller A (1970) J Phys Chem 74:4473
4. Barbara PF, Brus LE, Rentzepis PM (1980) J Am Chem Soc 102:5631
5. Mishra AK, Dogra SK (1985) Bull Chem Soc Jpn 58:3587
6. Becker RS, Lenolele C, Zein A (1987) J Phys Chem 91:3509
7. Lamansky S, Djurovich P, Murphy D, Abdel-Razzaq F, Kwong R, Tsyba I, Bortz M, Mui B, Bau R, Thompson ME (2001) Inorg Chem 40:1704
8. Lamansky S, Djurovich P, Murphy D, Abdel-Razzaq F, Lee HF, Adachi C, Burrows PE, Forrest SR, Thompson ME (2001) J Am Chem Soc 123:4304
9. Brooks J, Babayan Y, Lamansky S, Djurovich PI, Tsyba I, Bau R, Thompson ME (2002) Inorg Chem 41:3055
10. Segal G, Pople JA (1966) J Chem Phys 44:3289
11. Casida ME, Jamorski C, Casida KC, Salahub DR (1998) J Chem Phys 108:4439
12. Nakatsuji H, Hirao K (1978) J Chem Phys 68:2053
13. Nakatsuji H (1978) Chem Phys Lett 59:362
14. Nakatsuji H (1979) Chem Phys Lett 67:329
15. Nakatsuji H (1992) Acta Chim Acad Sci Hung 129:719

16. Nakatsuji H, Kitao O, Yonezawa T (1985) J Chem Phys 83:723
17. Wan J, Hada M, Ehara M, Nakatsuji H (2001) J Chem Phys 114:5117
18. Wan J, Meller J, Hada M, Ehara M, Nakatsuji H (2000) J Chem Phys 113:7853
19. Poolmee P, Ehara M, Hannongbua S, Nakatsuji H (2005) Polymer 46:6474
20. Saha B, Ehara M, Nakatsuji H (2007) J Phys Chem A 111:5473
21. Fukuda R, Nakatsuji H (2008) J Chem Phys 128:094105
22. Becke AD (1988) Phys Rev A 38:3098
23. Becke AD (1993) J Chem Phys 98:1372
24. Lee C, Yang W, Parr RG (1988) Phys Rev B 37:785
25. Krishnan R, Binkley JS, Seeger R, Pople JA (1980) J Chem Phys 72:640
26. McLean AD, Chandler GS (1980) J Chem Phys 72:5639
27. Foresman JB, Head-Gordon M, Pople JA (1992) J Phys Chem 96:135
28. Dunning TH Jr, Hay PJ (1976) In: Schaefer HF III (ed) Modern theoretical chemistry, vol 2. Plenum, New York
29. Frisch MJ, Trucks GW, Schlegel HB, Scuseria GE, Robb MA, Chesseman JR et al (2004) Gaussian 03. Gaussian Inc., Wallingford
30. Nakatsuji H (1973) J Am Chem Soc 95:345
31. Nakatsuji H, Koga T (1981) The force concept in chemistry. Van Nostrand Reinhold, New York
32. Krumholz P (1951) J Am Chem Soc 73:3487
33. Pohlers G, Virdee S, Scaiano JC, Sinta R (1996) Chem Matter 8:2654
34. Burrell GJ, Hurtubise RJ (1988) Anal Chem 60:2178
35. Drefahl G, Engelmann U (1960) Chem Ber 93:492
36. Gruzinskii VV, Danilova VI, Kopylova TN, Maier VG, Shalaev VK (1981) Sov J Quantum Electron 11:1029